

# Cobalt Phosphotungstate-Based Composites as Bifunctional Electrocatalysts for Oxygen Reactions

Ndrina Limani <sup>1,2</sup>, Inês S. Marques <sup>1</sup>, Bruno Jarrais <sup>1,\*</sup>, António J. S. Fernandes <sup>3</sup>, Cristina Freire <sup>1</sup> and Diana M. Fernandes <sup>1,\*</sup>

<sup>1</sup> REQUIMTE-LAQV/Departamento de Química e Bioquímica, Faculdade de Ciências, Universidade do Porto, 4169-007 Porto, Portugal; ndrinalimani@gmail.com (N.L.); up201608306@edu.fc.up.pt (I.S.M.); acfreire@fc.up.pt (C.F.)

<sup>2</sup> Université Paris Saclay, CEA, CEA Saclay, CNRS, NIMBE, LICSEN, F-91191 Gif Sur Yvette, France

<sup>3</sup> Departamento de Física, Instituto de Nanoestruturas, Campus Universitário de Santiago, Nanomodelação e Nanofabricação (I3N), Universidade de Aveiro, 3810-193 Aveiro, Portugal; toze2@ua.pt

\* Correspondence: bruno.jarrais@fc.up.pt (B.J.); diana.fernandes@fc.up.pt (D.M.F.)

## 1. Experimental section

### 1.1. Materials

**Table S1.** Samples code throughout manuscript and respective composition.

Sample Code	Sample Content
MWCNT	Pristine MWCNT
MWCNT_N8	MWCNT doped with nitrogen using melamine and 800 °C
MWCNT_N8_Co4	MWCNT_N8 with Co-POM
GF	Pristine graphene flakes
GF_N8	Graphene flakes doped with nitrogen using melamine and 800 °C
GF_ND8	Graphene flakes doped with nitrogen using dicyandiamide and 800 °C
GF_NS8	Graphene flakes doped with nitrogen and sulphur using dithioxamide and 800 °C
GF_N8_Co4	GF_N8 with Co-POM
GF_ND8_Co4	GF_ND8 with Co-POM
GF_NS8_Co4	GF_NS8 with Co-POM

### 1.2. Characterization Methods

The micro-Raman analysis was conducted in the backscattering configuration on a Jobin Yvon HR800 instrument (Horiba, Japan), using a 600 lines/mm grating and the 532 nm laser line from a Nd:YAG DPSS laser (Ventus, Laser Quantum, U.K.). For the Rayleigh rejection, a pair of edge filters placed in series was used allowing Raman acquisition from 50 cm<sup>-1</sup>. A 100× objective (spot size < 2 μm, numeric aperture = 0.9, Olympus, Japan) was used to focus the laser light onto the sample and to collect the backscattered Raman radiation to be detected by a Peltier cooled (223 K) CCD sensor. The spectrometer was operated in the confocal mode, setting the iris to 300 μm. The analysis were conducted at Centro de Investigação em Materiais Cerâmicos e Compósitos – CICECO – Universidade de Aveiro (Aveiro, Portugal).

A Jasco FT/IR-460 Plus spectrophotometer was used to acquire the Fourier transform infrared (FTIR) spectra (64 scans, resolution of 4 cm<sup>-1</sup> and between 400 and 4000 cm<sup>-1</sup>). The spectra were obtained for samples dispersed in KBr pellets (spectroscopic grade, Merck) comprising 0.2% of prepared composites.

X-ray photoelectron spectroscopy (XPS) measurements were performed at the Centro de Materiais da Universidade do Porto (CEMUP), Portugal, on A VG Scientific ESCALAB 200A spectrometer with non-monochromatized Al K $\alpha$  radiation (1486.6 eV) was used for X-ray photoelectron spectroscopy (XPS) measurements at CEMUP. Potential deviations induced by electric charge of the samples were corrected using the C 1s band at 284.6 eV as an internal standard. The analysis of XPS results were performed using the CasaXPS software for spectra

deconvolution. Surface atomic percentages were calculated from the corresponding peak areas upon spectra deconvolution and using the sensitivity factors provided by the manufacturer.

Scanning electron microscopy/Energy-dispersive X-ray spectroscopy (SEM/EDS) was carried out using a high resolution (Schottky) environmental SEM with X-ray microanalysis and electron backscattered diffraction analysis (Quanta 400 FEG ESEM/EDAX Genesis X4M), in high-vacuum conditions, at the Centro de Materiais da Universidade do Porto (CEMUP).

### 1.3. Assessment of Electrochemically Active Surface Areas (ECSA)

ECSA values exhibited by electrocatalysts are usually calculated by using the Equation (S1):

$$\text{ECSA} = C_{dl} / C_{ref} \quad (\text{S1})$$

where  $C_{dl}$  stands for the double-layer capacitance and  $C_{ref}$  for the reference capacitance value per unit area. Due to the impossibility of knowing the exact  $C_{ref}$  value for specific and structurally complex materials, reliable ECSA values cannot be obtained frequently. However, the linear proportional relation between ECSA and double-layer capacitance allows performing a relative comparison for similar electrocatalysts. Taking advantage of this fact, in the present work,  $C_{dl}$  values have been directly employed as approximated ECSA estimations to assess the surface effects on the OER performances. Thus,  $C_{dl}$  values were calculated for all materials via standard double-layer charging test, namely, acquisition of consecutive CV plots at different scan rates (from 20 to 160 mV s<sup>-1</sup>), being the double-layer capacitance estimated from the slope of linear-fitted plot of current density at 0.95 V vs. RHE (non-faradaic region) versus the scan rate.

### 1.4. ORR and Oer Electrochemical Performance

Both the CV and LSV measurements were performed between  $E_p = 0.26$  and 1.46 V vs. RHE at 0.005 V s<sup>-1</sup>. Additionally, rotation speeds in the range 400 - 3000 rpm were used for the LSV experiments. For the chronoamperometry (CA) tests a rotation speed of 1600 rpm for 20 000 s at a potential = 0.55 V vs. RHE was used. Tolerance to methanol was assessed by CA at  $E = 0.55$  V vs. RHE and 1600 rpm for 2500 s.

The effective ORR current was obtained by subtracting the current obtained in N<sub>2</sub>-saturated electrolyte by that obtained in O<sub>2</sub>-saturated.

Even though the potential were measured against the Ag/AgCl reference electrode these were converted to the reversible hydrogen electrode (RHE) using the Equation (S2) for a proper comparison with the literature results.

$$E_{(\text{RHE})} = E_{(\text{Ag/AgCl})} + 0.059 \text{ pH} + E^{\circ}_{(\text{Ag/AgCl})} \quad (\text{S2})$$

where  $E_{(\text{RHE})}$  is the potential vs. RHE,  $E^{\circ}_{(\text{Ag/AgCl})} = 0.1976$  V (25 °C) and  $E_{(\text{Ag/AgCl})}$  is the potential measure vs. Ag/AgCl<sup>1</sup>.

Onset potential ( $E_{\text{onset}}$ ) is defined as the potential at which the reduction of O<sub>2</sub> begins. According to literature the  $E_{\text{onset}}$  can be determined by different methods<sup>1-3</sup> and is generally assumed as the potential at which the ORR current is 5% of the diffusion-limiting current density or it can be calculated as the potential at which the slope of the voltammogram exceeds a threshold value ( $j = 0.1$  mA cm<sup>-2</sup>V<sup>-1</sup>)<sup>2,3</sup>. Here we considered the first method.

The kinetic parameters and the number of electrons transferred per O<sub>2</sub> molecule ( $n_{O_2}$ ) in the oxygen reduction reaction were determined using the following Koutecky-Levich equations:

$$\frac{1}{j} = \frac{1}{j_L} + \frac{1}{j_k} = \frac{1}{B\omega^{1/2}} + \frac{1}{j_k} \quad (\text{S3})$$

$$B = 0.2 n_{O_2} F (D_{O_2})^{2/3} v^{-1/6} C_{O_2} \quad (\text{S4})$$

Here,  $j$  is the current density measured,  $j_L$  and  $j_k$  are the diffusion-limiting and kinetic current densities,  $\omega$  is the angular velocity,  $F$  is the Faraday constant (96 485 C mol<sup>-1</sup>),  $D_{O_2}$  is the O<sub>2</sub> diffusion coefficient (1.95×10<sup>-5</sup> cm<sup>2</sup> s<sup>-1</sup>),  $v$  is the electrolyte kinematic viscosity (0.008977 cm<sup>2</sup> s<sup>-1</sup>),  $C_{O_2}$  is the O<sub>2</sub> bulk concentration (1.15×10<sup>-3</sup> mol dm<sup>-3</sup>). For rotation speeds in rpm is adopted a constant of 0.2<sup>4</sup>.

Tafel plots were obtained after the measured LSV currents were corrected for diffusion to yield the corresponding kinetic current values. The  $j_L$  parameter, obtained through the combination of Equations (S3) and (4), was used to make the mass transport correction. The values of  $j_k$  obtained were normalized for the total deposited mass of EC.

Rotating ring disk electrode (RRDE) measurements in O<sub>2</sub>-saturated KOH solution were also performed in order to obtain a more in-depth insight of the ORR electrocatalytic activity of the ECs. The H<sub>2</sub>O<sub>2</sub> yields were determined from the ring and disk currents ( $i_R$  and  $i_D$ , respectively), and the current collection efficiency of the Pt ring ( $N = 0.25$ , in this case) using Equation (S5)<sup>5</sup>:

$$\% \text{ H}_2\text{O}_2 = 200 \times \frac{i_R/N}{i_D + i_R/N} \quad (\text{S5})$$

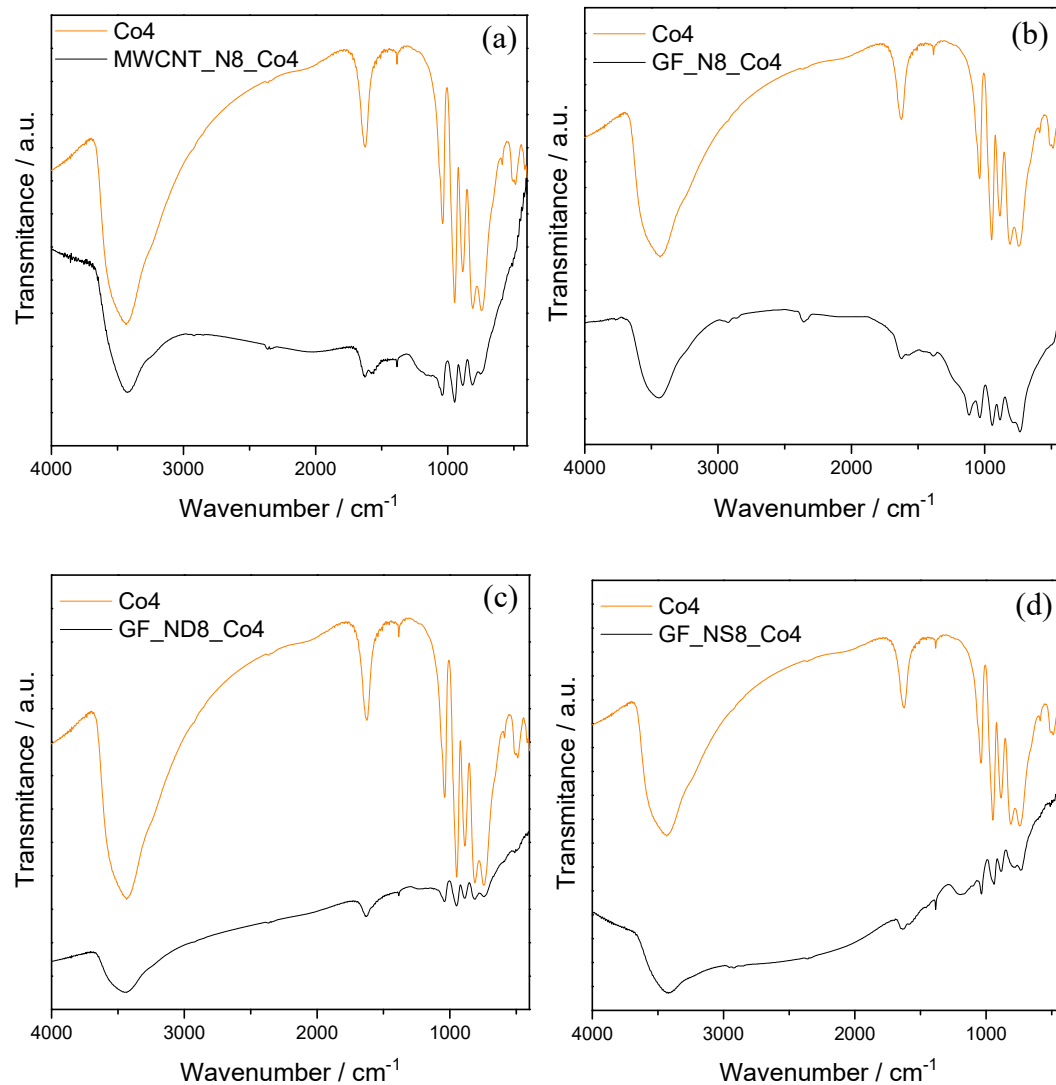
OER studies were performed in N<sub>2</sub>-saturated alkaline electrolyte, 0.1 M KOH solution purged with N<sub>2</sub> for at least 30 min before the measurement. LSVs were obtained by sweeping the potential from 0.87 to 1.87 V (vs. RHE) with a scan rate of 0.005 V s<sup>-1</sup> at 1600 rpm. All presented LSV tests were performed with  $i_R$ -compensation, via previous calculation of the uncompensated resistance (Ru) of the circuit by using  $i$ -interrupt approach, and finally, applying an  $i_R$ -compensation value equal to 0.90×Ru to the LSV measurement. Tafel slopes were determined by linear fitting of LSV data to the following equation:

$$\eta = a + b \times \log |j| \quad (\text{S6})$$

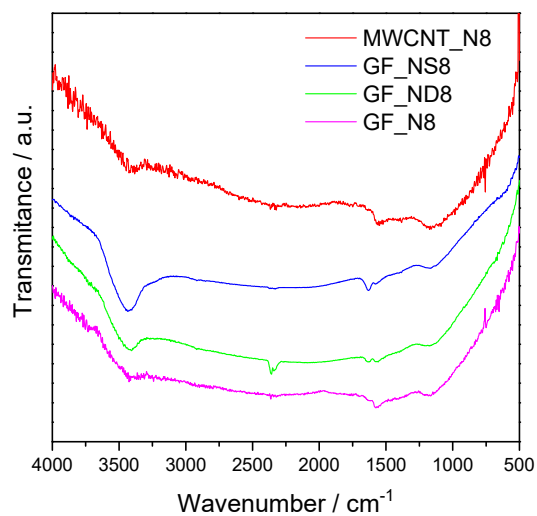
where  $\eta$  is the overpotential,  $b$  is the Tafel slope, and  $j$  is the current density.

## 2. Results and Discussion

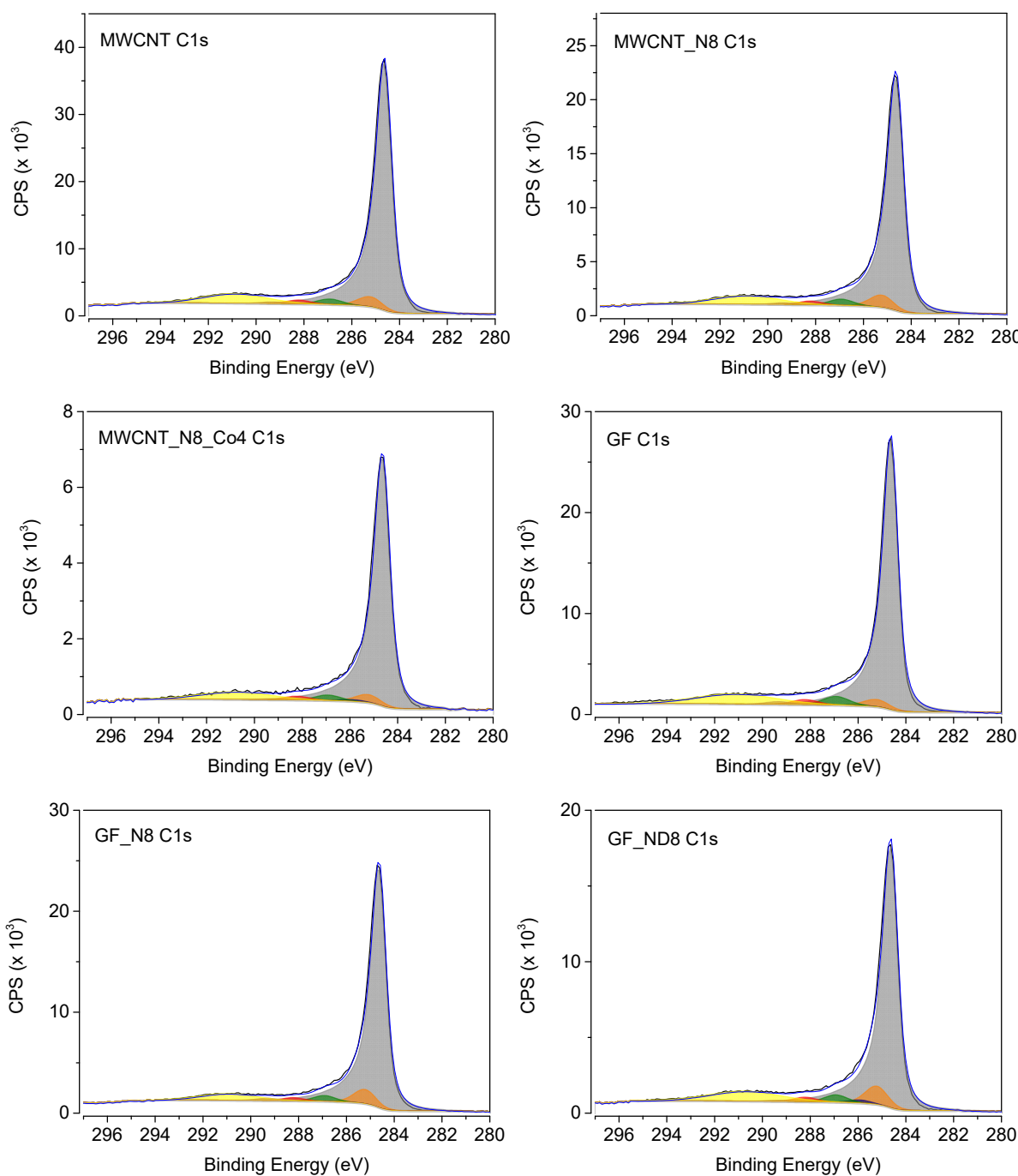
### 2.1. Materials Characterization



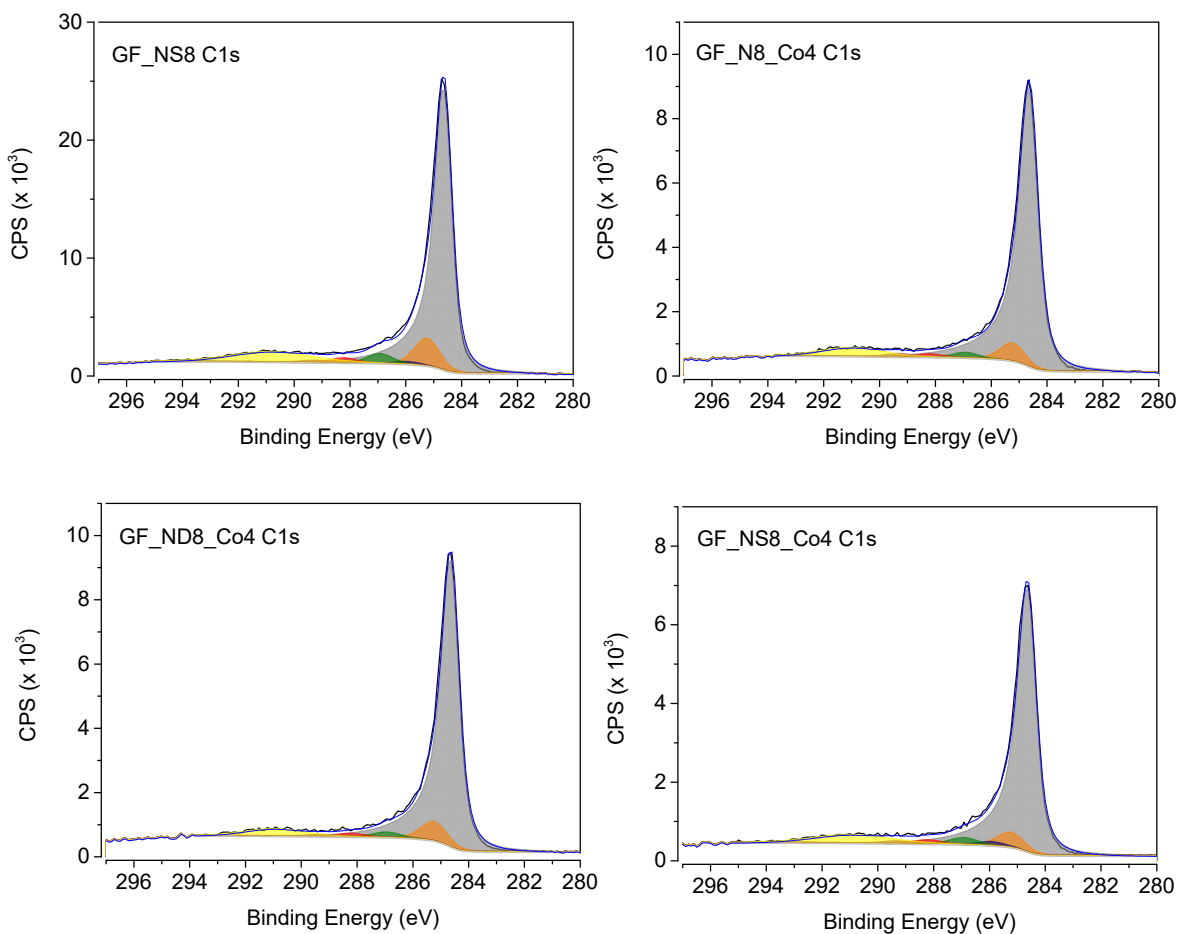
**Figure S1.** FTIR spectra of MWCNT\_N8\_Co4 (a), GF\_N8\_Co4 (b), GF\_ND8\_Co4 (c), and GF\_NS8\_Co4 (d).



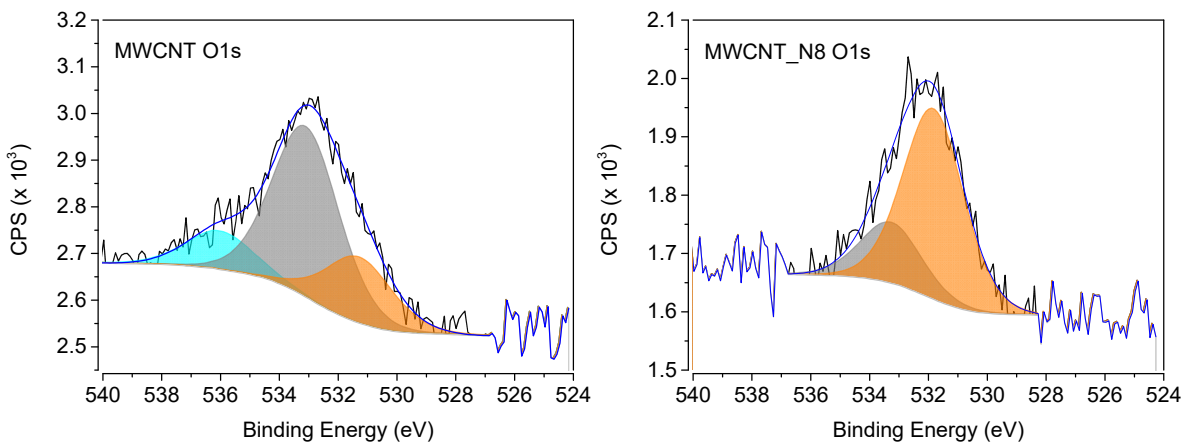
**Figure S2.** FTIR spectra of MWCNT\_N8, GF\_N8, GF\_ND8 and GF\_NS8.



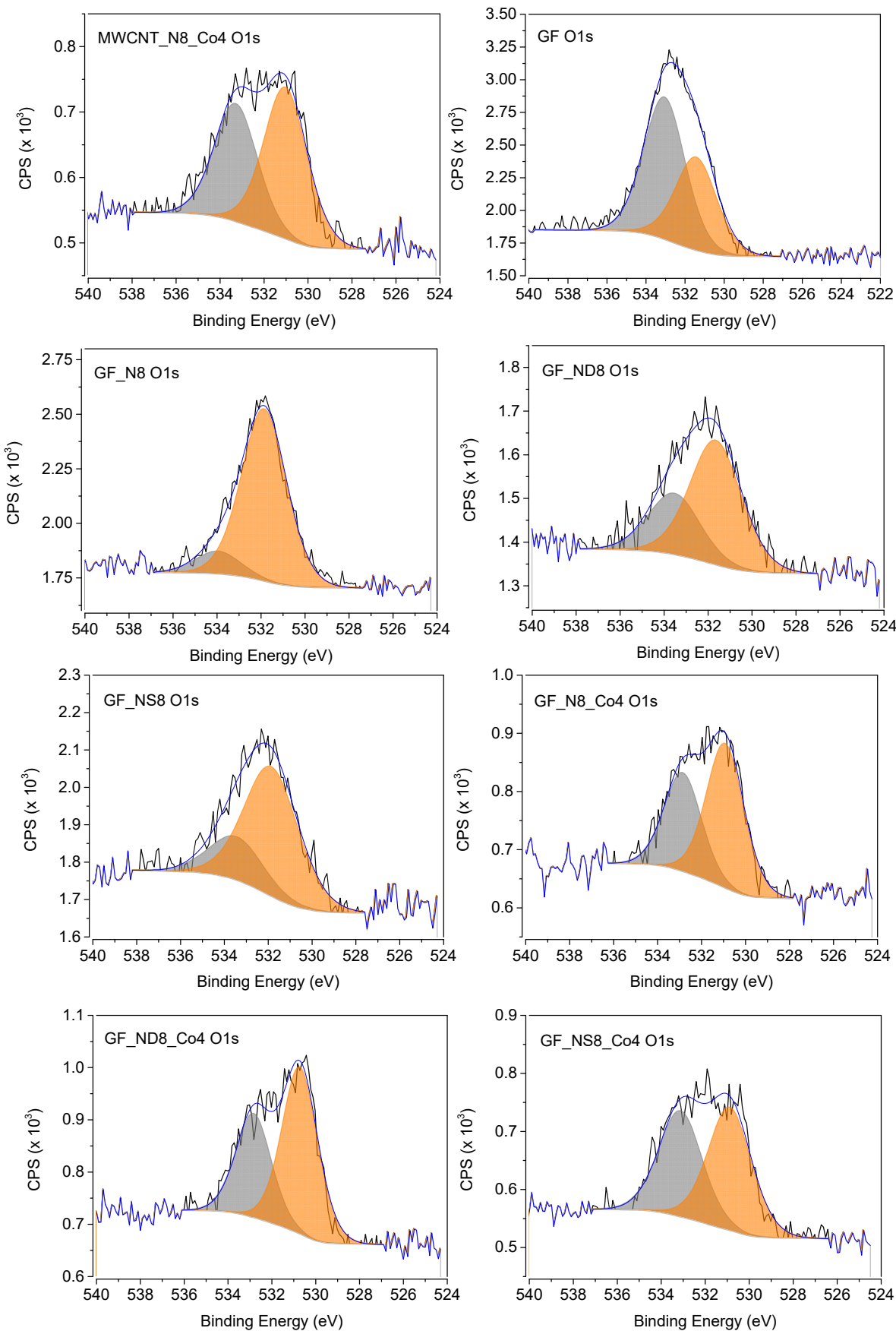
**Figure S3.** Deconvoluted C1s high resolution spectra of MWCNT- and GF-based materials.

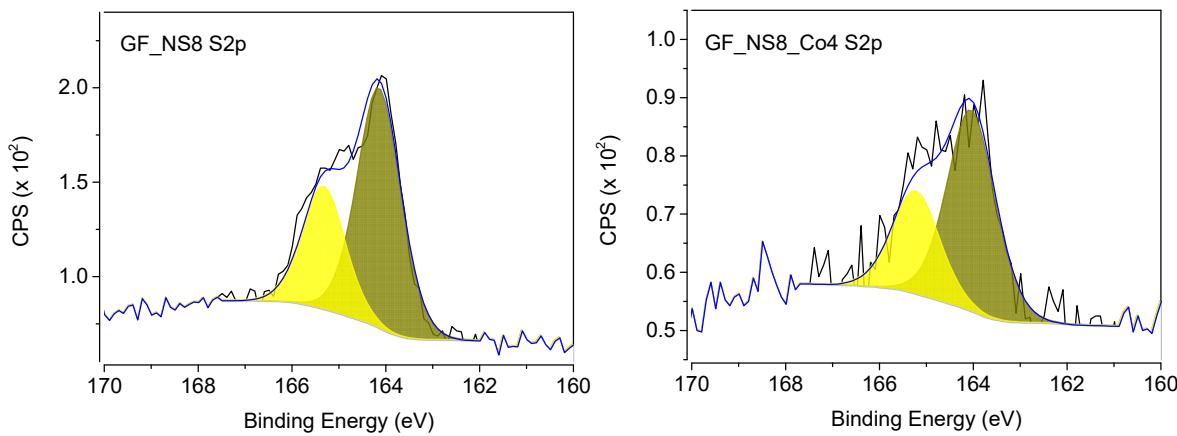
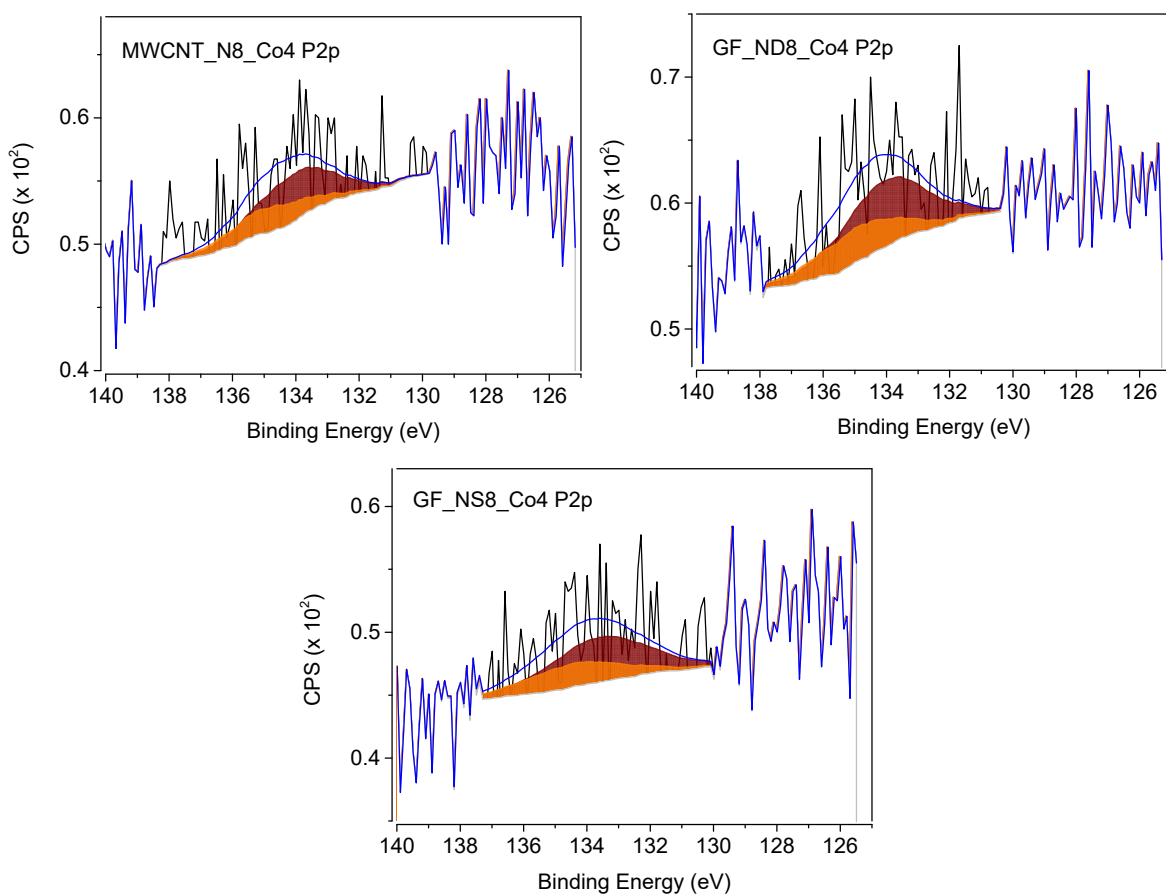


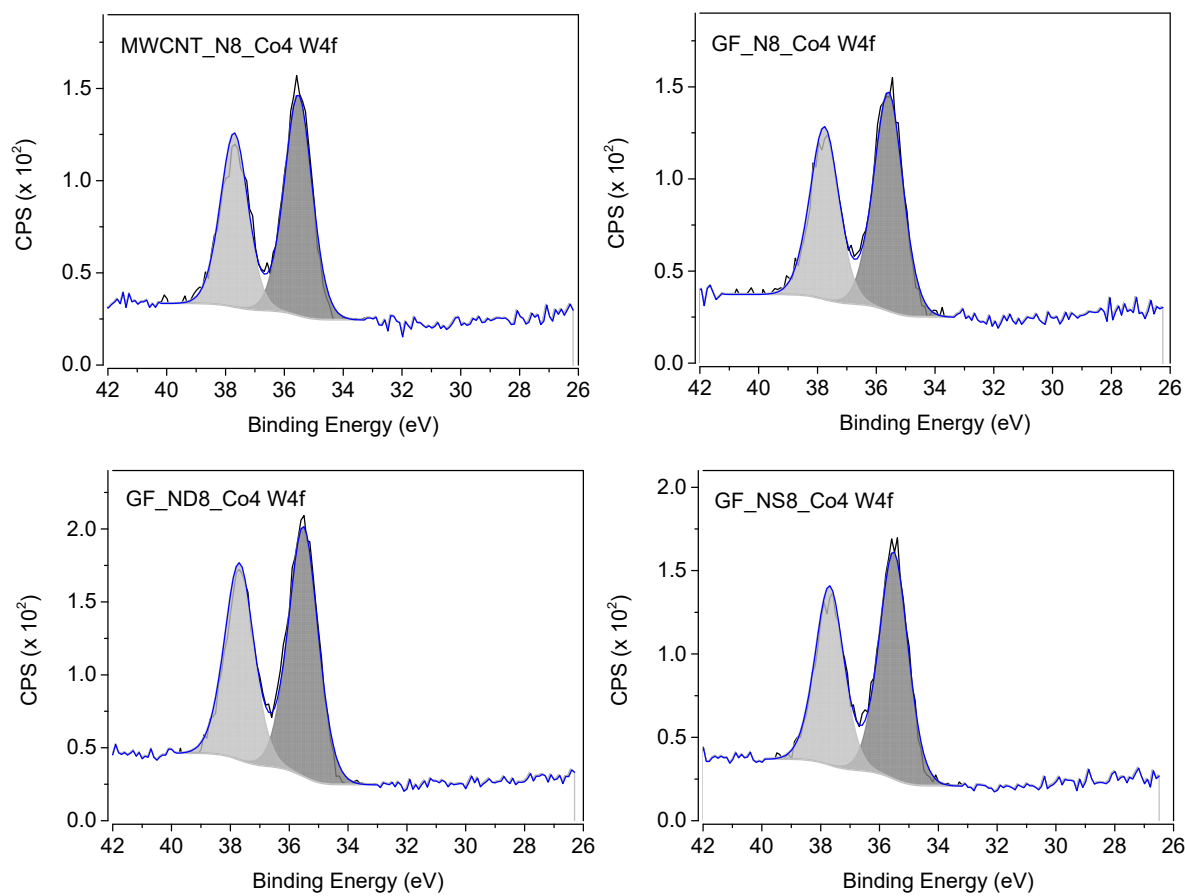
**Figure S3. (cont.).** Deconvoluted C1s high resolution spectra of MWCNT- and GF-based materials.



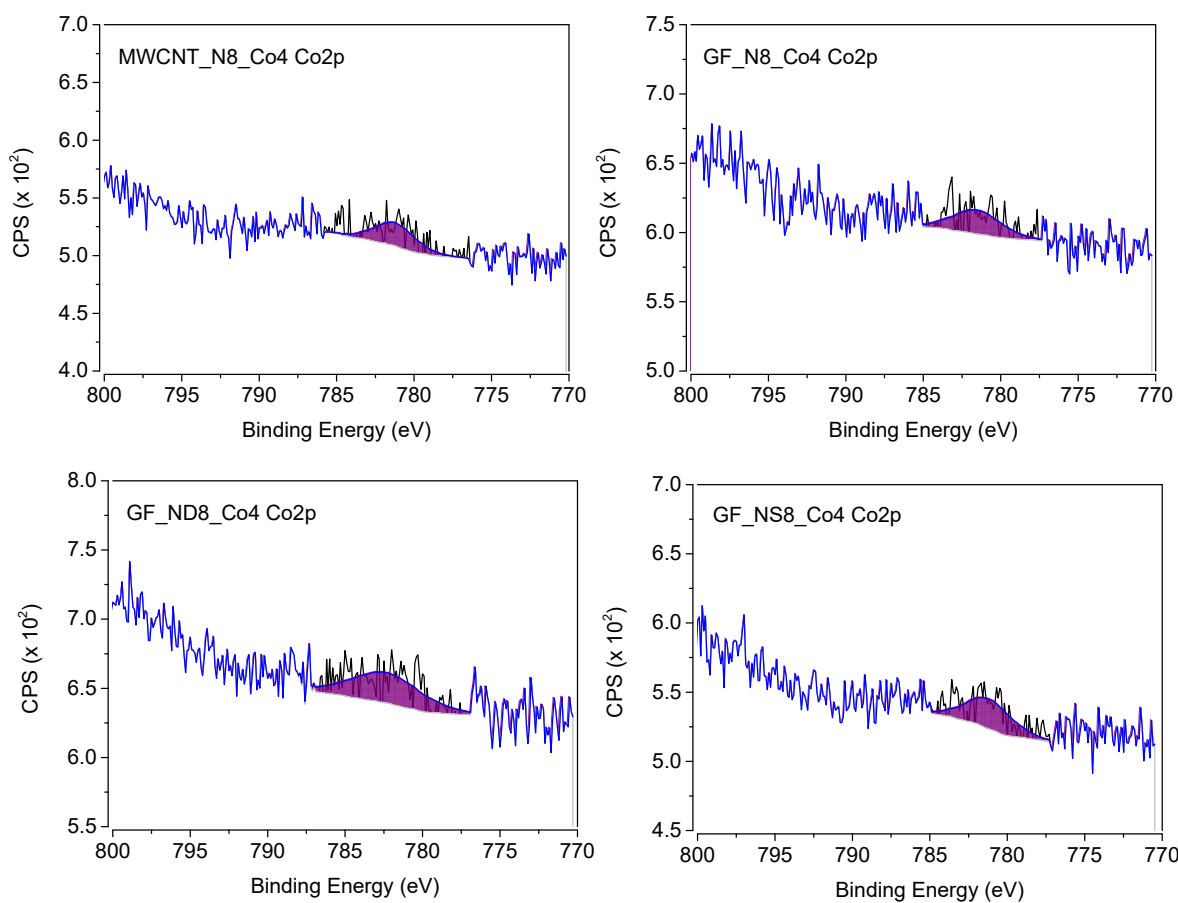
**Figure S4.** Deconvoluted O1s high resolution spectra of MWCNT- and GF-based materials.



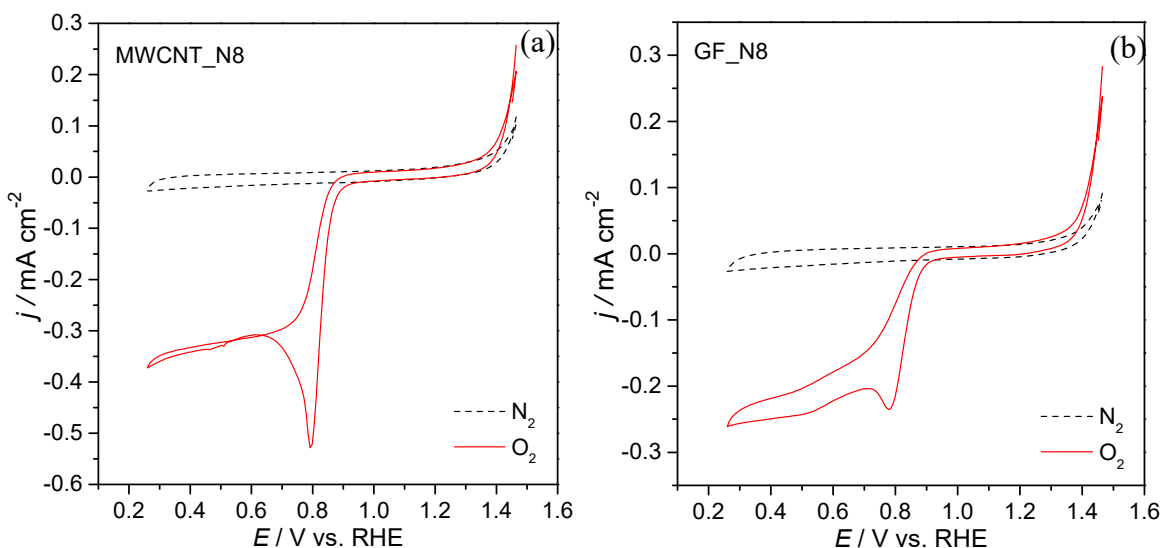
**Figure S4. (cont.).** Deconvoluted O1s high resolution spectra of MWCNT- and GF-based materials.**Figure S5.** Deconvoluted S2p high resolution spectra of GF\_NS8 and GF\_NS8\_Co4 materials.**Figure S6.** Deconvoluted P2p high resolution spectra of MWCNT\_N8\_Co4, GF\_ND8\_Co4, and GF\_NS8\_Co4 materials.

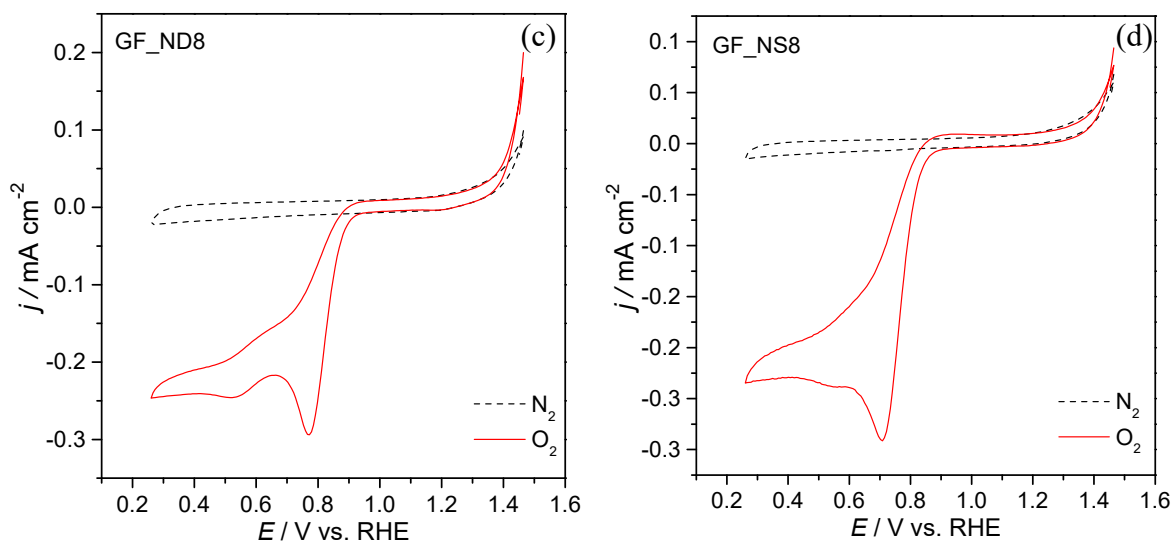


**Figure S7.** Deconvoluted W4f high resolution spectra of MWCNT\_N8\_Co4, GF\_ND8\_Co4, and GF\_NS8\_Co4 materials.

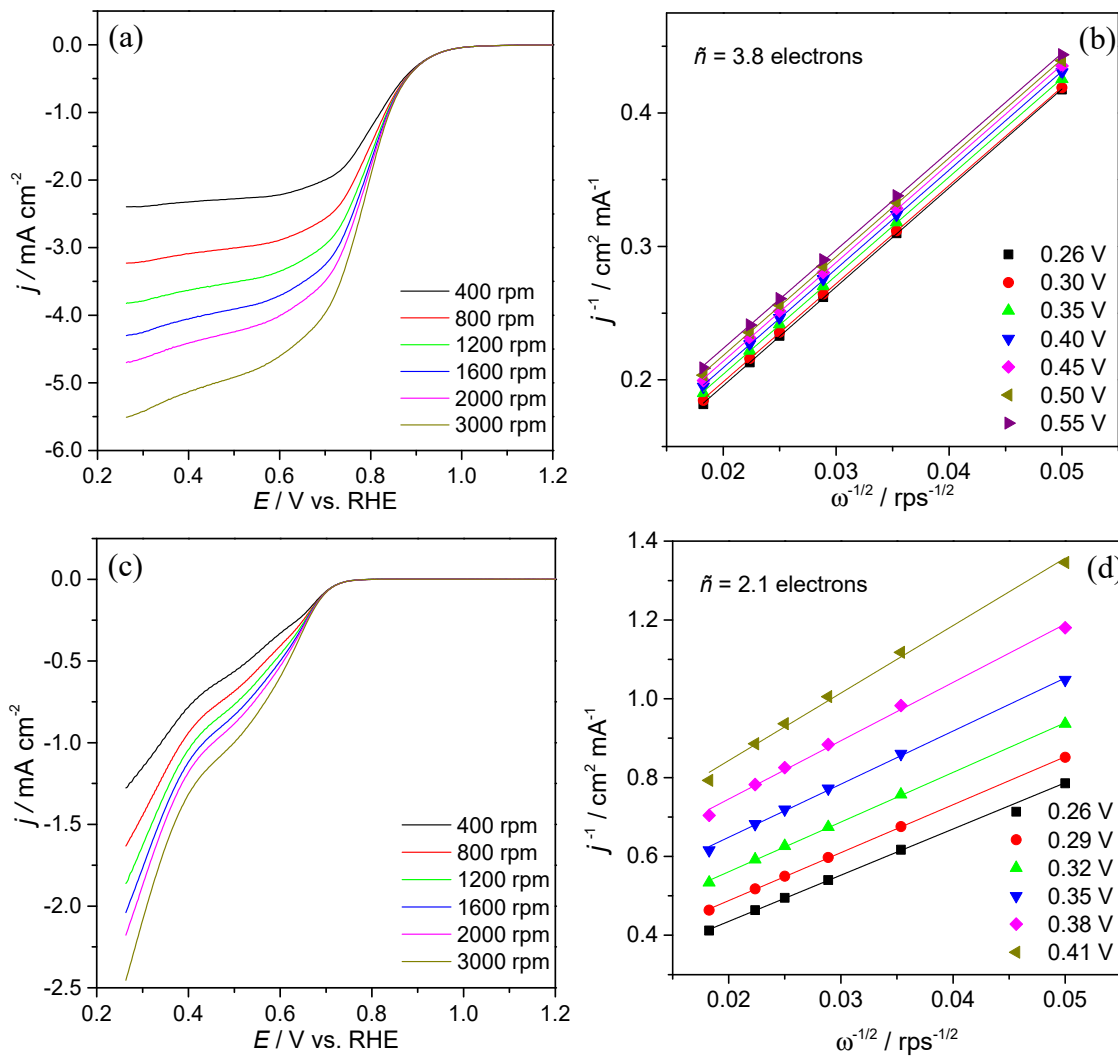


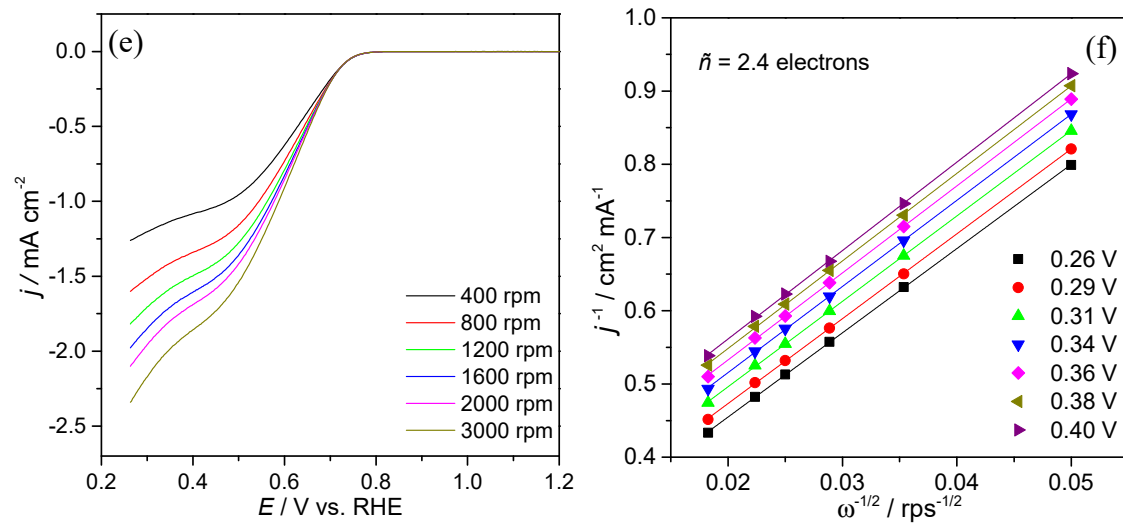
**Figure S8.** Deconvoluted Co2p high resolution spectra of MWCNT\_N8\_Co4, GF\_N8\_Co4, GF\_ND8\_Co4, and GF\_NS8\_Co4 materials.



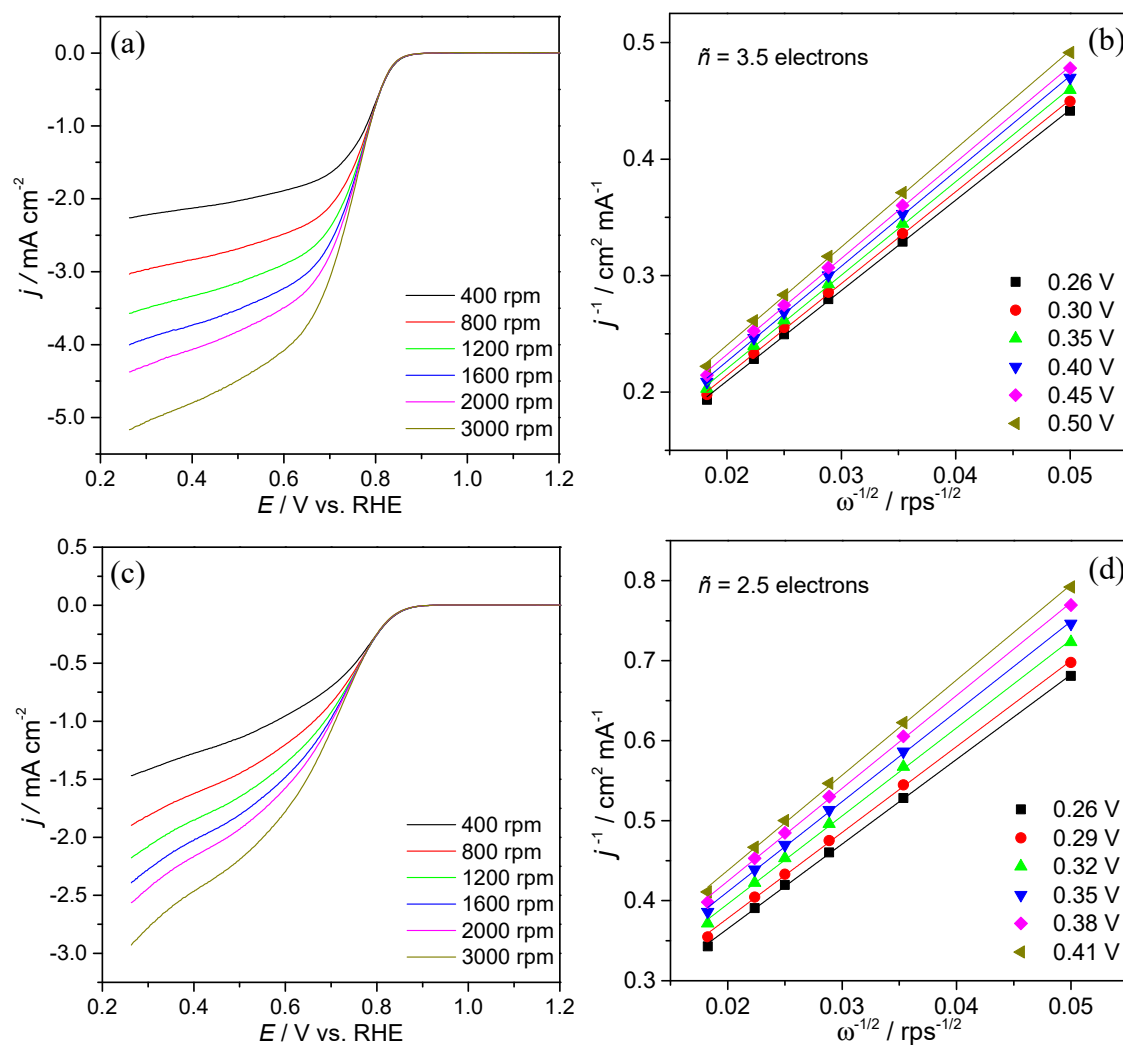


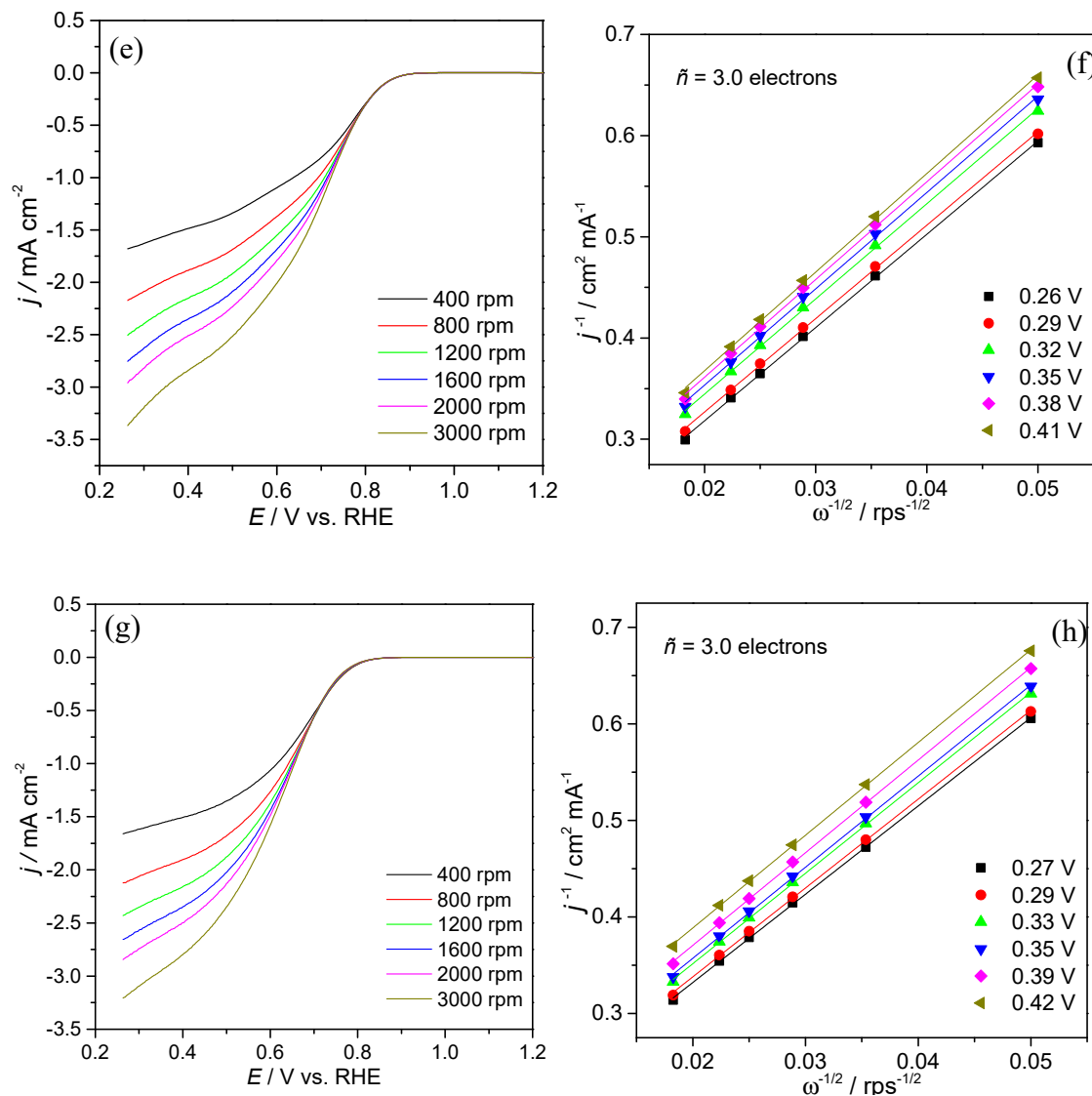
**Figure S9.** CVs of doped-CM/RDE in KOH (0.1 M) saturated in N<sub>2</sub> (dash line) and O<sub>2</sub> (red line) at 5 mV s<sup>-1</sup>.



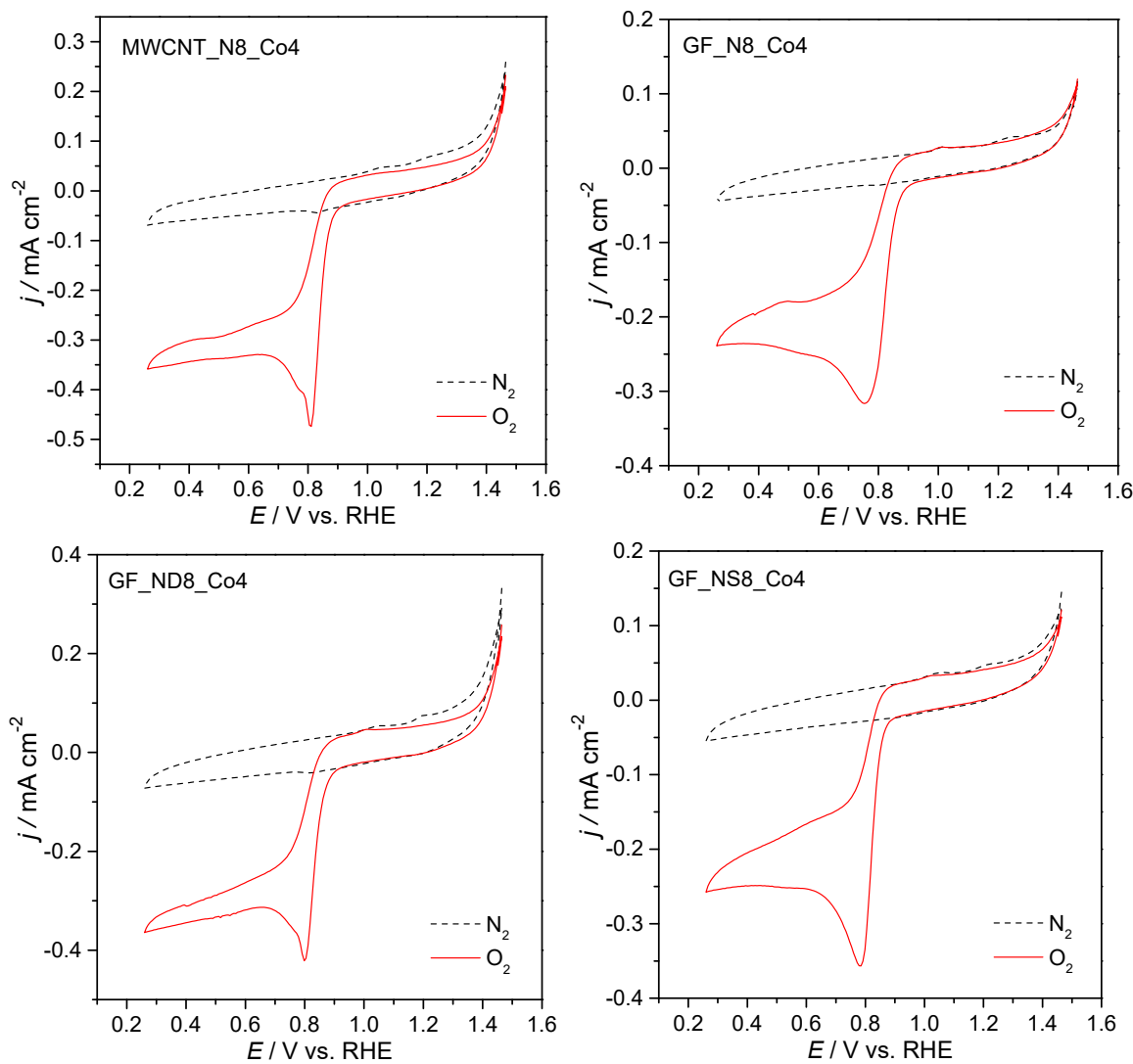


**Figure S10.** ORR polarization curves of Pt/C (a), pristine MWCNT (c) and pristine GF (e) modified electrodes, acquired at different rotation rates in  $O_2$ -saturated  $0.1 \text{ mol dm}^{-3}$  KOH solution at  $0.005 \text{ V s}^{-1}$  and the corresponding Koutecky-Levich (K-L) plots (b, d and f).

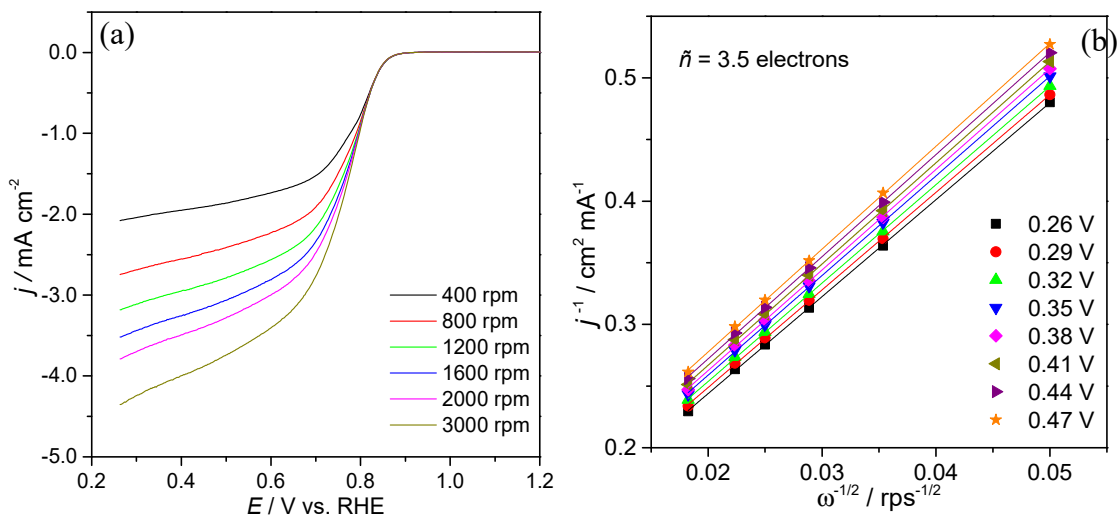


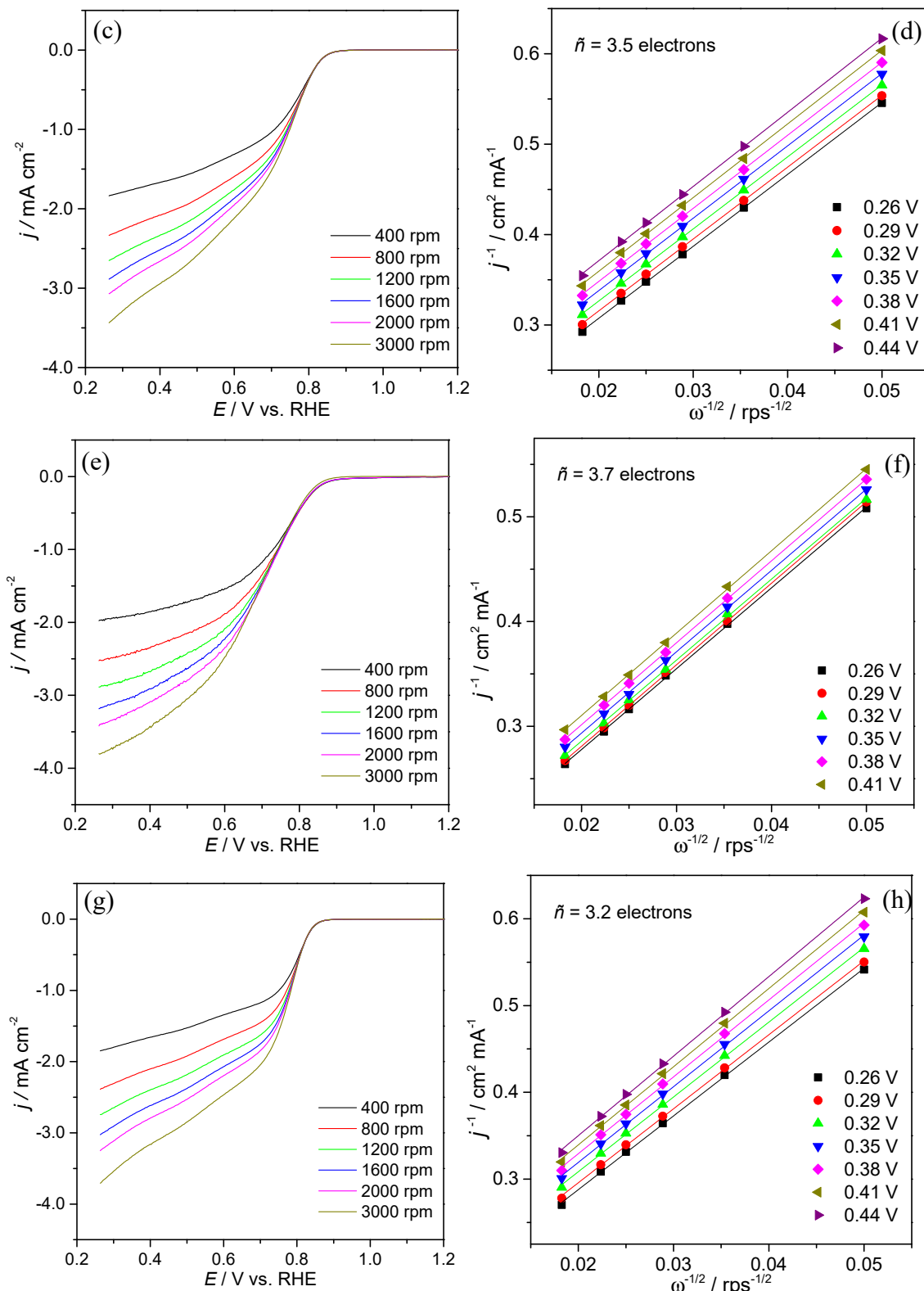


**Figure S11.** ORR polarization curves of MWCNT\_N8 (a), GF\_N8 (c) GF\_ND8 (e) and GF\_NS8 (g) modified electrodes, acquired at different rotation rates in O<sub>2</sub>-saturated 0.1 mol dm<sup>-3</sup> KOH solution at 0.005 V s<sup>-1</sup> and the corresponding Koutecky-Levich (K-L) plots (b, d, f and h).

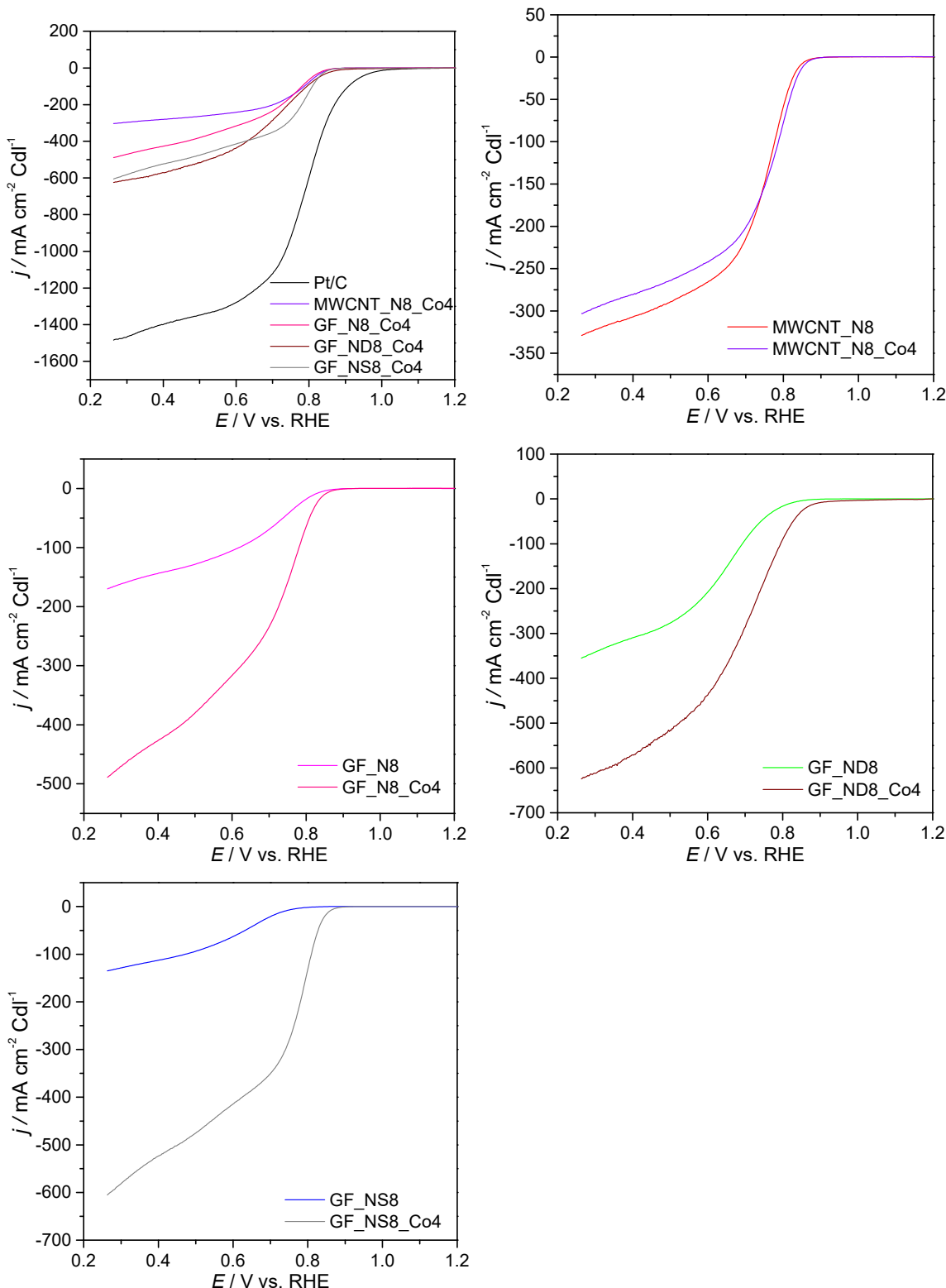


**Figure S12.** CVs of Co4@doped-CM/RDE in KOH (0.1 M) saturated in  $\text{N}_2$  (dash line) and  $\text{O}_2$  (red line) at  $5 \text{ mV s}^{-1}$ .

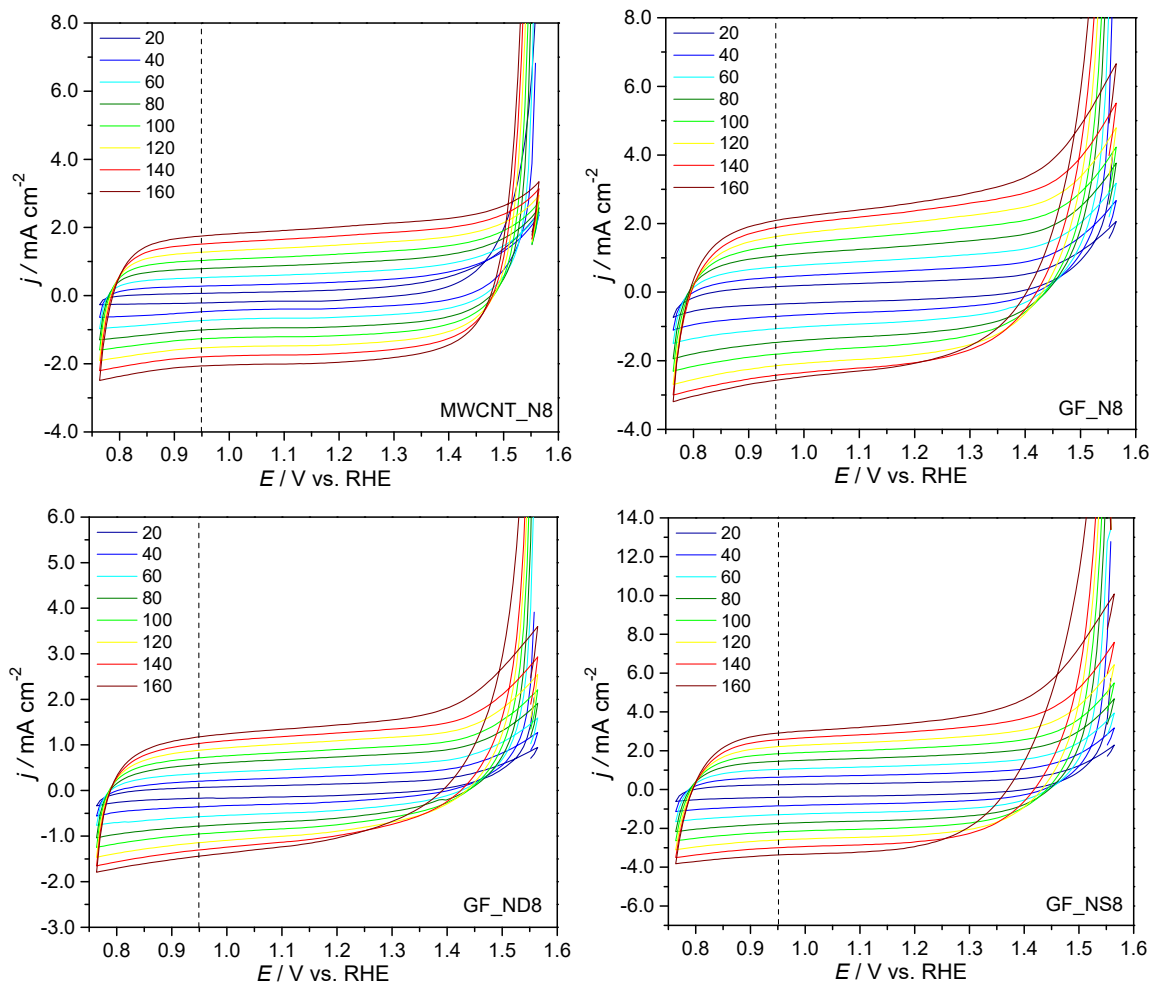




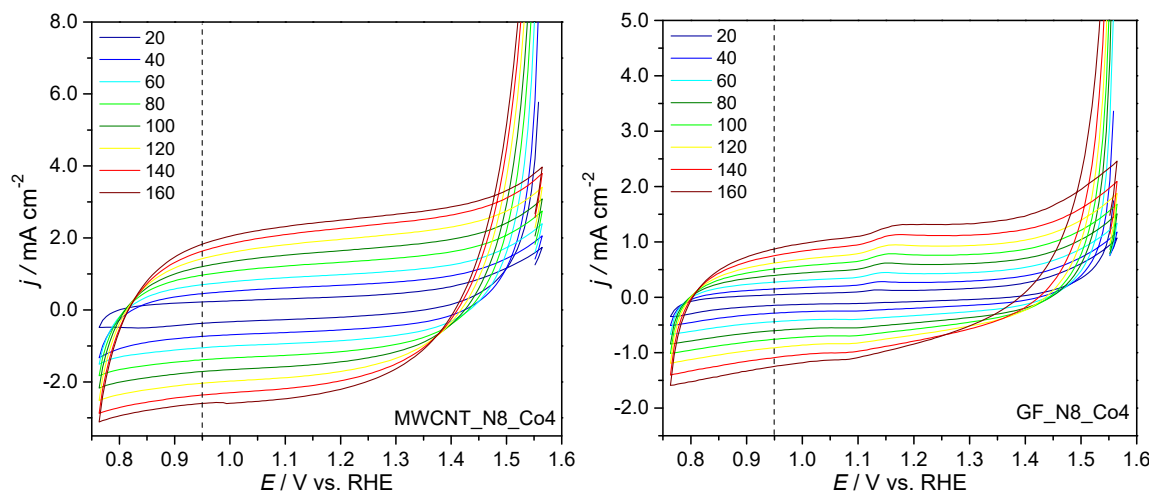
**Figure S13.** ORR polarization curves of MWCNT\_N8\_Co4 (a), GF\_N8\_Co4 (c) GF\_ND8\_Co4 (e) and GF\_NS8\_Co4 (g) modified electrodes, acquired at different rotation rates in  $\text{O}_2$ -saturated  $0.1 \text{ mol dm}^{-3}$  KOH solution at  $0.005 \text{ V s}^{-1}$  and the corresponding Koutecky-Levich (K-L) plots (b, d, f and h).

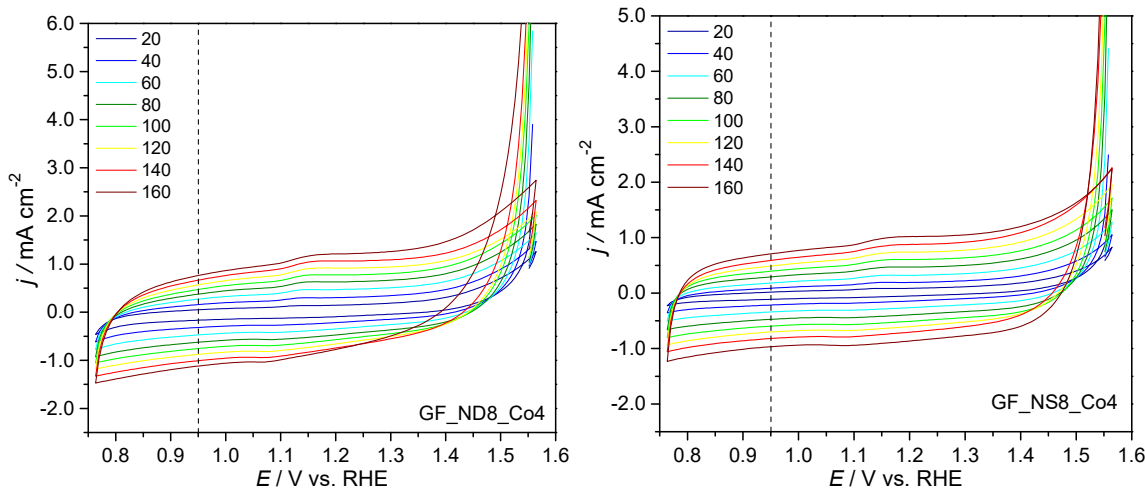


**Figure S14.** ORR LSV curves obtained in KOH (0.1 M) saturated with O<sub>2</sub> at 1600 rpm and 0.005 V s<sup>-1</sup> with current densities normalized to the respective double-layer capacitance values.

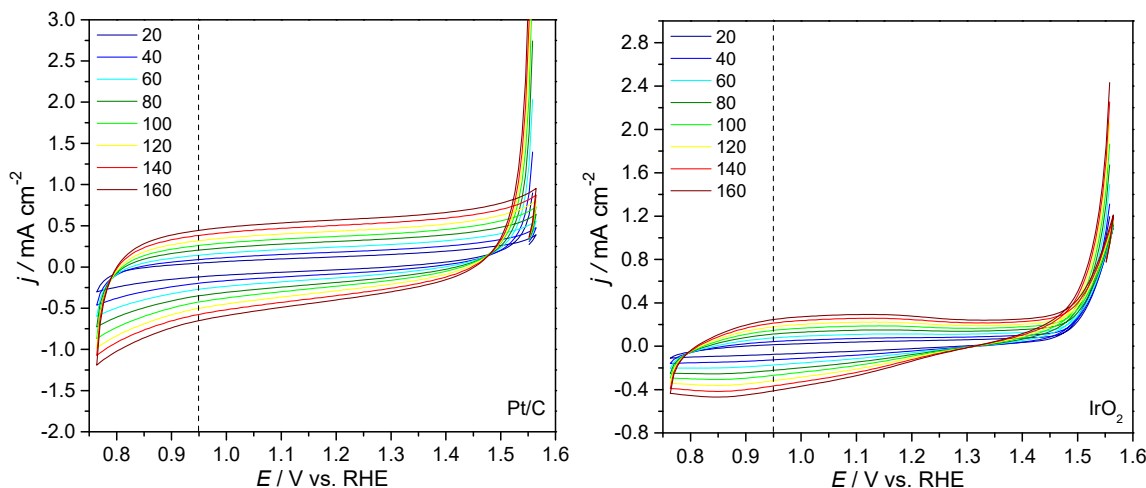


**Figure S15.** CVs at different scan rates of doped-CM/RDE in  $\text{N}_2$ -saturated KOH (0.1 M).

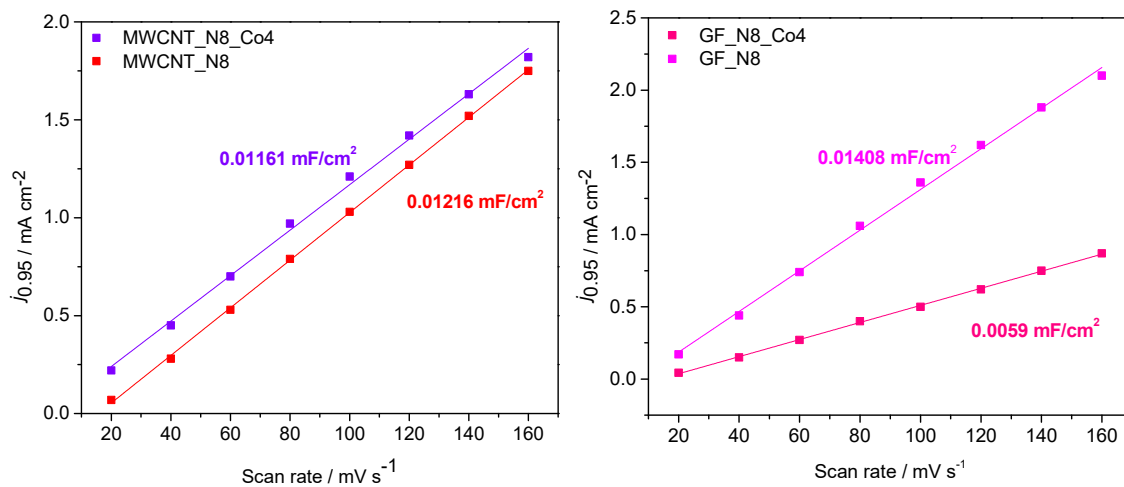




**Figure S16.** CVs at different scan rates of Co4@doped-CM/RDE in N<sub>2</sub>-saturated KOH (0.1 M).



**Figure S17.** CVs at different scan rates of Pt/C and IrO<sub>2</sub> in N<sub>2</sub>-saturated KOH (0.1 M).



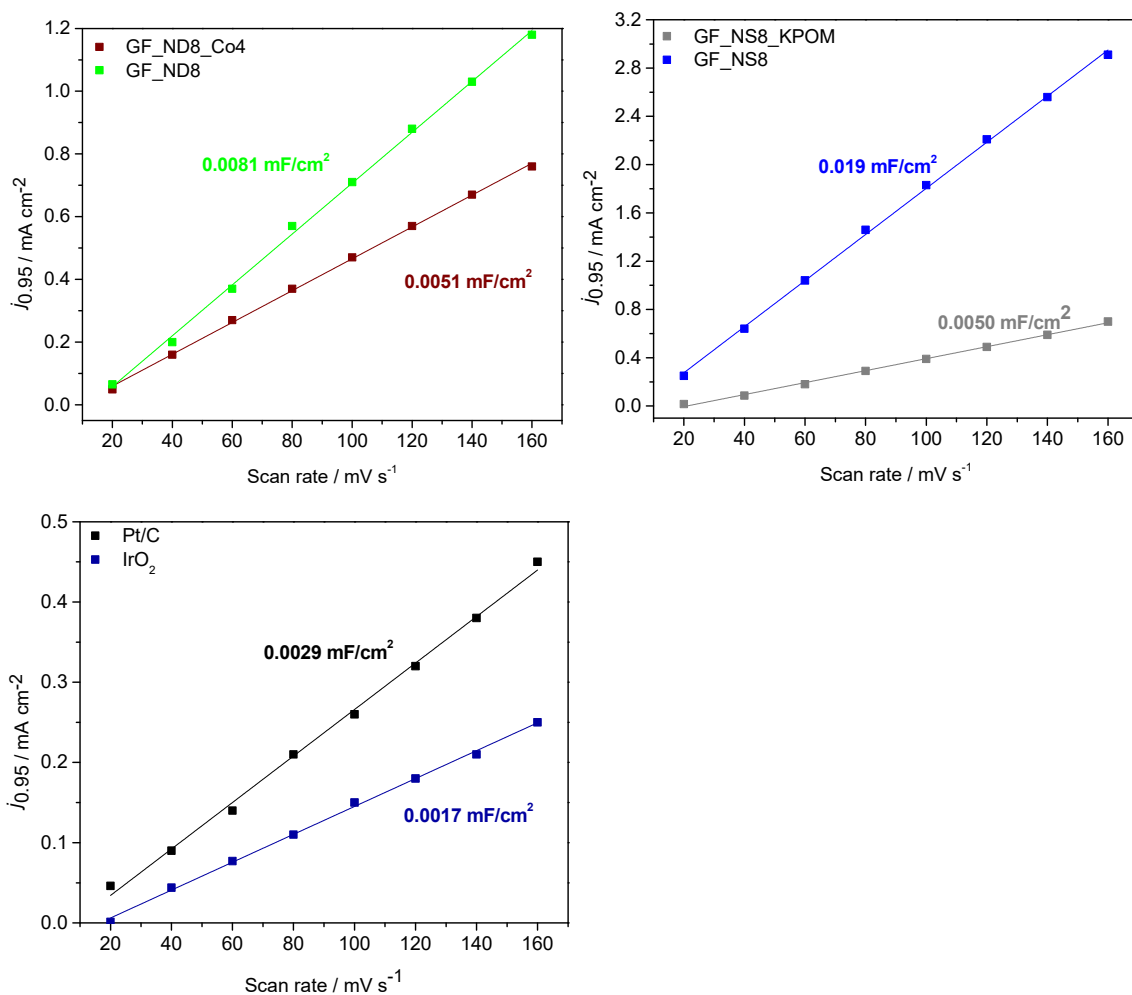


**Figure S18.** Current density-scan rate linear fitting plots for all materials. Numeric values correspond to double-layer capacitances ( $C_{dl}$ ) for each material.

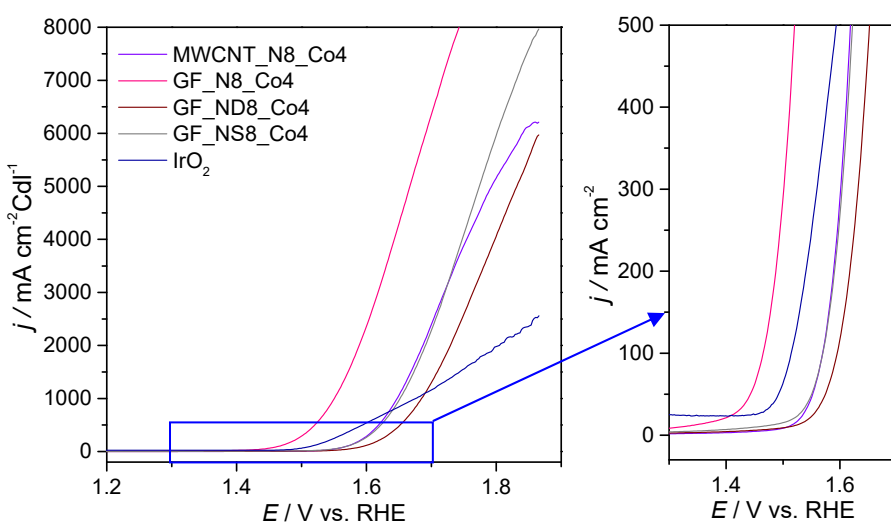


**Figure S19.** OER LSV curves obtained in KOH (0.1 M) saturated with  $\text{N}_2$  at 1600 rpm and  $0.005 \text{ V s}^{-1}$  with current densities normalized to the respective double-layer capacitance values.

**Table S2.** Relative atomic percentages of carbon-containing groups from the deconvolution of the C 1s high resolution XPS spectra of the carbon materials.

Sample	Atomic %						
	284.6 eV (sp <sup>2</sup> C)	285.2 eV (sp <sup>3</sup> C, C-X) <sup>a</sup>	285.9 eV (C-X, C-Y) <sup>a</sup>	286.9 eV (C-O-C)	288.2 eV (C=O)	289.3 eV (COOH)	291.0 eV (π→π*)
MWCNT	82.2	3.9	-	2.1	1.5	0.7	9.6
MWCNT_N8	81.2	4.8	-	2.5	1.5	0.7	9.3
MWCNT_N8_Co4	83.1	3.3	0.7	2.3	1.6	0.3	8.7
GF	78.5	2.8	0.3	3.3	2.0	1.1	12.0
GF_N8	83.5	5.5	-	2.2	1.3	0.9	6.6
GF_ND8	78.1	6.1	1.0	2.4	1.5	0.4	10.3
GF_NS8	76.7	8.1	0.8	2.8	1.4	0.6	9.6
GF_N8_Co4	84.8	5.4	-	1.6	0.9	0.9	6.4
GF_ND8_Co4	85.1	6.2	0.1	1.7	1.1	0.6	5.2
GF_NS8_Co4	81.4	5.0	1.3	2.3	1.3	0.9	7.8

<sup>a</sup> X = N and/or X = S; Y = OH.

**Table S3.** Onset potentials ( $E_{\text{onset}}$ ), diffusion-limiting current density ( $j_{\text{L}}$ ) and the number of electrons transferred per O<sub>2</sub> molecule for carbon-based materials containing Co-POMs or other cobalt materials reported in literature.

Sample	$E_{\text{onset}}$ vs. RHE	$\tilde{n}$	$j_{\text{L}}$ (mA cm <sup>-2</sup> )	Reference
Co/N <sub>3</sub> S <sub>3</sub> -GF	0.87	4.0	-3.98	5
Co <sub>3</sub> O <sub>4</sub> @g-C <sub>3</sub> N <sub>4</sub> /NG	0.92	≈3.9	≈ -5.0	6
N-rGO/CNT/Co <sub>3</sub> O <sub>4</sub>	0.87	≈4.0	≈ -4.0	7
Co <sub>4</sub> (PW <sub>9</sub> ) <sub>2</sub> @SWCNT	0.77	3.9	-3.2	8
Co <sub>4</sub> (PW <sub>9</sub> ) <sub>2</sub> @GF	0.89	2.7	-3.3	8
Co <sub>4</sub> (PW <sub>9</sub> ) <sub>2</sub> @N-CNT	0.90	4.0	-8.5	8
Co <sub>4</sub> (PW <sub>9</sub> ) <sub>2</sub> @N-FLG	0.89	3.6	-4.4	8

## References

1. Freire, C.; Fernandes, D.M.; Nunes, M.; Abdelkader, V.K. POM & MOF-based Electrocatalysts for Energy-related Reactions. *ChemCatChem* **2018**, *10*, 1703–1730.
2. Daems, N.; Sheng, X.; Vankelecom, I.F.J.; Pescarmona, P.P. Metal-free doped carbon materials as electrocatalysts for the oxygen reduction reaction. *J. Mater. Chem. A* **2014**, *2*, 4085–4110.
3. Zhou, X.J.; Qiao, J.L.; Yang, L.; Zhang, J.J. A Review of Graphene-Based Nanostructural Materials for Both Catalyst Supports and Metal-Free Catalysts in PEM Fuel Cell Oxygen Reduction Reactions. *Adv. Energy Mater.* **2014**, *4*, 25.
4. Tuci, G.; Zafferoni, C.; Rossin, A.; Milella, A.; Luconi, L.; Innocenti, M.; Phuoc, L.T.; Cuong, D.V.; Cuong, P.H.; Giambastian, G. Chemically Functionalized Carbon Nanotubes with Pyridine Groups as Easily Tunable N-Decorated Nanomaterials for the Oxygen Reduction Reaction in Alkaline Medium. *Chem. Mater.* **2014**, *26*, 3460–3470.
5. Fernandes, D.M.; Mathumba, P.; Fernandes, A.J.S.; Iwuoha, E.I.; Freire, C. Towards efficient oxygen reduction reaction electrocatalysts through graphene doping. *Electrochim. Acta* **2019**, *319*, 72–81.
6. Wang, Y.Q.; Yin, X.; Shen, H.B.; Jiang, H.; Yu, J.W.; Zhang, Y.F.; Li, D.W.; Li, W.Z.; Li, J.  $\text{Co}_3\text{O}_4@\text{g-C}_3\text{N}_4$  supported on N-doped graphene as effective electrocatalyst for oxygen reduction reaction. *Int. J. Hydrogen Energy* **2018**, *43*, 20687–20695.
7. Lu, H.Y.; Huang, Y.P.; Yan, J.J.; Fan, W.; Liu, T.X. Nitrogen-doped graphene/carbon nanotube/ $\text{Co}_3\text{O}_4$  hybrids: One-step synthesis and superior electrocatalytic activity for the oxygen reduction reaction. *RSC Adv.* **2015**, *5*, 94615–94622.
8. Fernandes, D.M.; Novais, H.C.; Bacsa, R.; Serp, P.; Bachiller-Baeza, B.; Rodriguez-Ramos, I.; Guerrero-Ruiz, A.; Freire, C. Polyoxotungstate@Carbon Nanocomposites As Oxygen Reduction Reaction (ORR) Electrocatalysts. *Langmuir* **2018**, *34*, 6376–6387.